J. Mater. Environ. Sci. 4 (4) (2013) 571-582
ISSN : 2028-2508
CODEN: JMESCN

New composites based on castor oil with isophorone diisocyanate polyurethanes and cellulose fibers

Ikram Ganetri [1,2], Lan Tighzert [2] , Philippe Dony [2], Allal Challioui [1*]

[1]*Laboratoire de Chimie Organique, Macromoléculaire et Produits Naturels – Equipe Photochimie & Chimie Macromoléculaire (PCM)- Faculté des Sciences – Université Mohamed Premier. BP: 717 – 60 000 Oujda – Maroc.*
[2]*Groupe de Recherche En Sciences Pour l'Ingénieur / Matériaux Fonctionnels (LISM) – Ecole Supérieure d'Ingénieurs de Reims (ESIReims), Esplanade Roland Garros – Pôle Henri-Farman, B.P.1029 – 51686 Reims Cedex 2, France.*

Received 10 Dec 2012, Revised 29 Mar 2013, Accepted 29 Mar 2013
* Corresponding author. E mail: a_challi@yahoo.fr; Tel

Abstract
Castor oil (**CO**) based polyurethanes (**IPU**) were synthesized and mixed to cellulose fibers extracted from Alfa plant to prepare composites with different cellulose contents (5, 10, 15, 20, 30 and 40 wt%). Films of the composites were characterized by thermal analysis and mechanical testing. FTIR spectra showed hydrogen bonding between urethane groups and hydroxyl groups of cellulose suggesting compatibility between polymer matrix and cellulose fibers as reveled by scanning electron microscopy (**SEM**). The influence of cellulose content on thermal stability and mechanical properties of the composites has been studied. The mechanical testing showed optimum value of Young modulus and elongation at break at 15%wt of cellulose content. Thermal properties show an increase in Tg value and char yield with the percentage of fibers. Besides, water uptake tests showed an increase in hydrophilicity of the composites with increasing fiber amount in the matrix and swelling test demonstrates higher crosslinking density with higher content of filler.

Keywords: Polyurethanes, castor oil, cellulose fibers, eco-friendly composites, physical properties.

1. Introduction
Recent years have witnessed an increasing demand of natural products in industrial applications for environmental issues, waste disposal, and depletion of non-renewable resources. Therefore, there has been a growing search for new materials with high performance at affordable costs. Nowadays, natural fiber reinforced polymer composites are of tremendous importance both in end-use applications and in the areas of research and development. Among the renewable natural resources, plant oils and vegetal fibers have been used for various applications such as coatings, inks, and agrochemicals [1-4].
Polyurethanes (**PUs**) are versatile polymers that have been extensively used in manufacturing products ranging from expanded to highly compact materials. The use of **PUs** has been proven viable in composite matrices for their flexibility and abrasion resistance [5-6]. Castor oil (**CO**) based **PUs** were extensively studied and widely used as starting materials for many industrial applications [7-8] such as paints, inks, coatings, lubricants. The chemistry of castor oil is centered on its high content of ricinoleic acid triglycerides and the hydroxyl functions which can react with isocyanate functions (Fig.1) to give polyurethane elastomers [9], interpenetrating polymer network [10], millable polyurethane [11], castable polyurethane [12], adhesives and coatings [13], and polyurethane foams [14].
However, oil based polymeric materials do not show properties of rigidity and strength required for structural applications by themselves [15]. The main disadvantages with the use of castor oil include low hydroxyl number and aliphatic structure leading to inherently soft materials [4]. To overcome these drawbacks, the reinforcement of castor oil based PUs matrices with cellulose fibers can lead to new composite materials with enhanced thermal and mechanical properties. In fact, cellulose fibers constitute an attractive alternative to the mineral fibers because of their economical production with few requirements for equipments and low density which makes it possible to obtain lighter composites, bio-renewable character, ubiquitous availability in a variety of forms [16-18].

Besides, these reinforcements are biodegradable and fit easily into the earth–ecological cycles. Thus, new materials and composites derived from natural sources rich in cellulose, and offering environmental and economic benefits, are being developed by the automotive, construction, household furniture, and packaging industries. Therefore, it is important to improve these materials for better and more effective use [19]. The aim of this paper is to present the results obtained in the synthesis of castor oil based composite materials and their thermal, mechanical and morphological characterization.

2. Materials and methods

2.1. Solvents and reagents

Castor oil (**CO**), 3-isocyanatomethyl-3,5,5-triméthylcyclohexyl isocyanate commonly known as isophorone diisocyanate 98% (**IPDI**)and dibutyl tin dilaurate (**DBTDL**) were obtained from Aldrich. Acetone was purchased from Charbonneaux (FRANCE). All reagents were used as received. The cellulose fibers were extracted from alfa stems using Kraft method in alkali medium. The structure of the cellulose fibers were confirmed by FTIR using a commercial sample as reference [20].

2.2. Apparatus

Infrared spectra were recorded by attenuated transmittance reflection–Fourier transform infrared mode with FTIR 8400 S SHIMADZU in a range of 4000 to 700 cm^{-1}. The samples were scanned 128 times.

Thermal properties were studied by differential scanning calorimetry (**DSC**) and thermogravimetric analysis (**TGA**). The **DSC** analyses were determined using DSC 204 F1 Pheonix NETZSCH (Germany). Around 15 mg of sample was placed in closed aluminum capsules. Each sample was subject to the heating/cooling cycle between -50 and 200°C with a scanning rate 10 °C/min. The glass transition temperatures T_g were taken at the midpoint (1/2 ΔCp) of the stepwise increasing of the heat capacity from the second scan curves. **TGA** thermograms were obtained using TG 209 F3 TARSUS NETZSCH 51 apparatus at a heating rate of 10°C/min from 25 to 700°C.

Morphology of the fractured surface of the films was investigated by scanning electron microscopy (**SEM**) using a microscope JEOL JSM-6460LA (Japan) equipped with an energy dispersive (Si-Li) X-ray spectrometer. The electron beam is incident on the specimen perpendicularly to the surface. All samples were frozen in liquid nitrogen and manually broken. Their facial fracture was analyzed.

Mechanical properties including tensile strength, Young's modulus and elongation at break were determined from stress–strain curves obtained with MTS Adamel Lhomargy- DY35XL tester at strain rate of 10 mm/min. All the presented data were averaged from seven replicates where the value of the confidence interval coefficient is $\alpha = 0.05$.

Water uptake (**WU**) of the composites was determined by immersing pre-dried samples in distilled water at 30°C during 30 days. Three samples were tested for each material type. After a time interval, the samples were removed from water, carefully blotted to remove the excess water on the surface, and immediately weighed. The WU percentage was calculated as:

$$\mathbf{WU = (mt\text{-}m_0/m_0)x100}$$

Where: m_0 and m_t are the sample weights before and after the immersion to distilled water for time "t", respectively.

The contact angle (**CA**) measurements were performed with Contact Angle System OCA APOLLO INSTRUMENTS Dataphysics. Sequences of 60 s were recorded after the deposition of 3 µl water drop. Teli OCD Camera image analysis software was used to determine the contact angle evolution. Swelling test was performed in pure toluene. Three samples were tested for each material type. The samples were weighted each 10 min until reaching a constant mass. The toluene uptake (%TU) was calculated as below:

$$\mathbf{\%TU = (mt\text{-}m_0/m_0)x100}$$

Where: m_0 and m_t are the sample weights before and after the immersion in toluene for time "t", respectively. The presented data are the average of tree replicate.

2.3. Polyurethane synthesis:

CO (30 g, 932 g/mol) and **IPDI** (16 g, 222.28 g/mol) were mixed in a flask equipped with a mechanical stirrer and a nitrogen inlet in the presence of DBTDL as catalyst at 0.05 wt% of **CO**. The reaction was carried out at 90°C for 2 hours in dry nitrogen atmosphere. The molar ratio of [**CO**]/[**NCO** groups] was 1/2.6. The obtained **PU** is referenced as **IPU**.

2.3. Preparation of cast films for mechanical and thermal characterization:
All the films were prepared by solution casting. Typical preparation was performed as follows: in small beakers equipped with magnetic stirrers, 4 g of **IPU** kept in the final stage of polymerization before gel point, and 20 ml of acetone were charged. The mixture is heated at 40°C and stirred until dilute dispersions were obtained, and then the desired amount of extracted cellulose fibers finely crushed and filtered through sieves with pore diameter of 40 µm were added. The dispersion solution was cast on a freshly cleaned glass. The composites were left at ambient temperature for 24 hours and then dried at 80°C for 48 hours. The films were kept in desiccators for future characterization.
The designation used for the prepared films are referenced in Table 1.

Table 1: Designation of the film composites elaborated by casting IPU and cellulose fibers.

Percentage of cellulose fibers	Designation of the film based on **IPU** (**IPUi**)
0%	**IPU100**
5%	**IPU95**
10%	**IPU90**
15%	**IPU85**
20%	**IPU80**
30%	**IPU70**
40%	**IPU60**

3. Results and discussion

3.1. Structural characterization:
The polyurethane matrix was synthesized by reacting **CO** with **IPDI** using a molar ratio [**NCO**]/[**OH**] = 1 (Fig. 1).

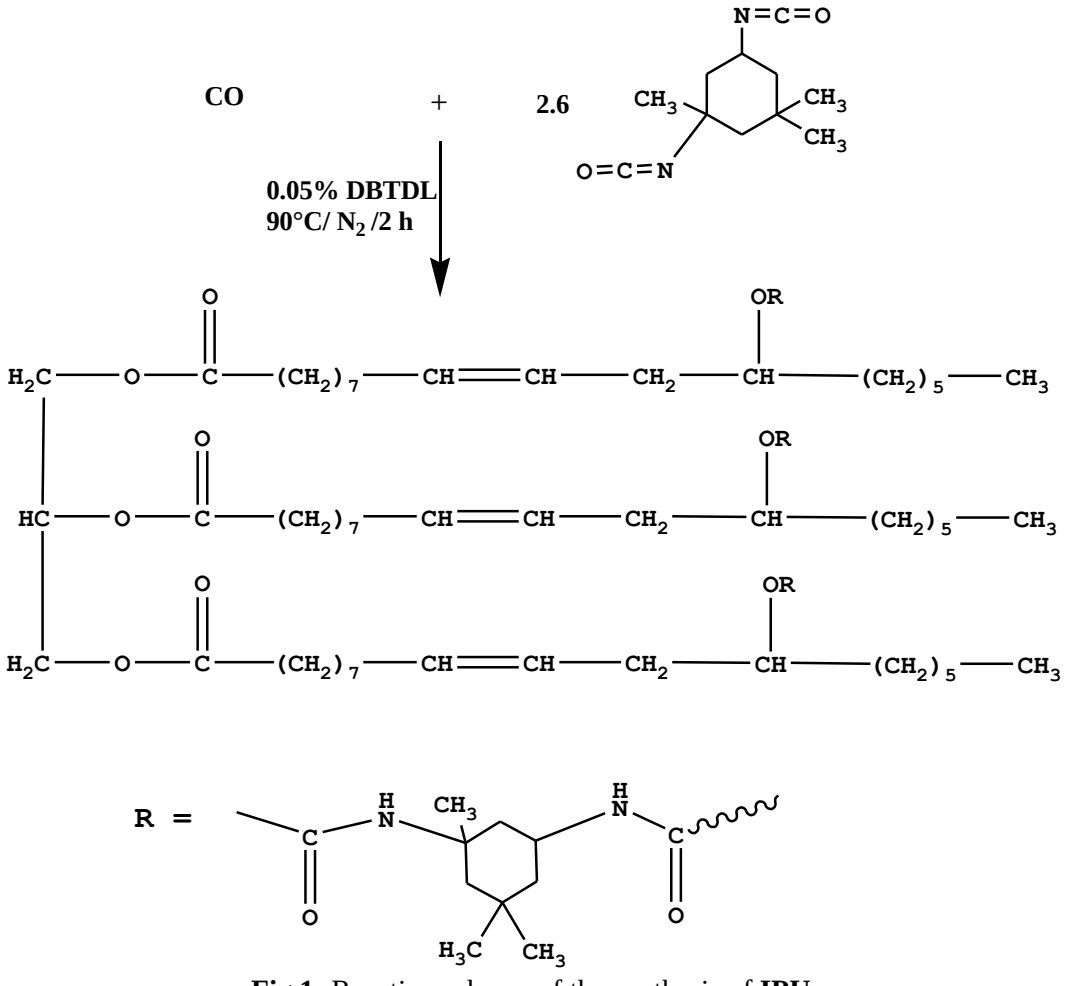

Fig.1: Reaction scheme of the synthesis of **IPU**.

The formation of urethane linkage were confirmed by FTIR spectroscopy of the final product IPU100 (Fig. 2) where the bands corresponding to isocyanate N=C=O and hydroxyl functions at 2245 cm^{-1} and 3425 cm^{-1} in **IPDI** and **CO** respectively, disappeared and new bands are observed. The first band at 3360 cm^{-1} is assigned to stretching vibration —N—H and the broad band between 1703 - 1699 cm^{-1} is attributed to the carbonyl group of the urethane linkage. Furthermore, the band at 1519 cm^{-1} is characteristic of the —C—N— of urethane group.

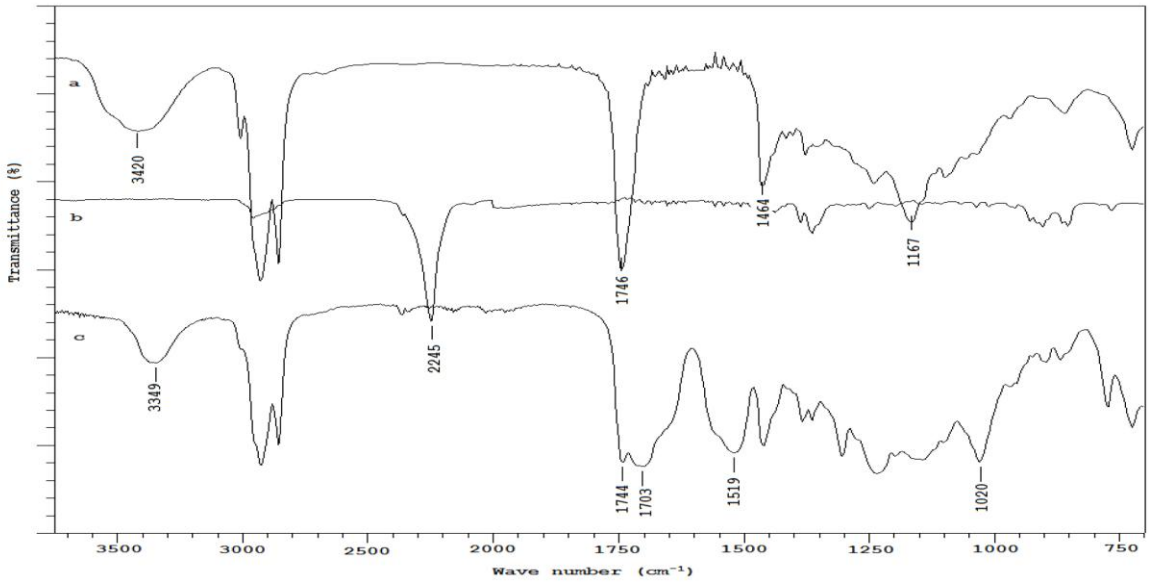

Fig.2: ATR-FTIR spectra of **CO** (a), **IPDI** (b) and **IPU100** (c).

The composites IPUi were prepared by mixing polyurethane matrix in its final stage of polymerization before the gel point and cellulose fibers finely crushed and filtered through sieves with pores of 40 µm. The content in renewable resources is higher than 60% in all the prepared composites (table 2) and therefore, they are potential candidate for biomaterial applications.

Table 2: content (weight %) of the prepared composites in isophorone di-isocyanate (**IPDI**).

Composite	IPDI weight percentage (%)
IPU100	38.60
IPU95	36.67
IPU90	34.74
IPU85	32.81
IPU80	30.88
IPU70	27.02
IPU60	23.16

Figure 3 shows the FTIR spectra of **CO**, cellulose and composites with different content of cellulose. The cellulose spectrum is characterized by the broad band between 3100 and 3600 cm^{-1} assigned to the hydroxyl groups [21], and the peak at 1030 cm^{-1} is characteristic of the vibration of C-O linkage in ether and alcohol functions of cellulose structure [22].

From the composites spectra, it can be seen that the bands corresponding to -N-H stretching (3360 cm^{-1} in IPU100) are shifted to lower wave numbers in the composites (3357 in IPU95, 3350 cm^{-1} in IPU80 and 3341 cm^{-1} in IPU60). The greater is the percentage of cellulose in composite; the lower is the wave number of -N-H vibration (table 3).

The so called red shift of the N–H stretching vibration provides unambiguous information about the formation of hydrogen bonds [23]. Moreover, this peak is larger in composites than in IPU100, confirming the presence of hydrogen bonding between N—H groups of urethane functions and both ether and hydroxyl groups of cellulose [24 – 25].

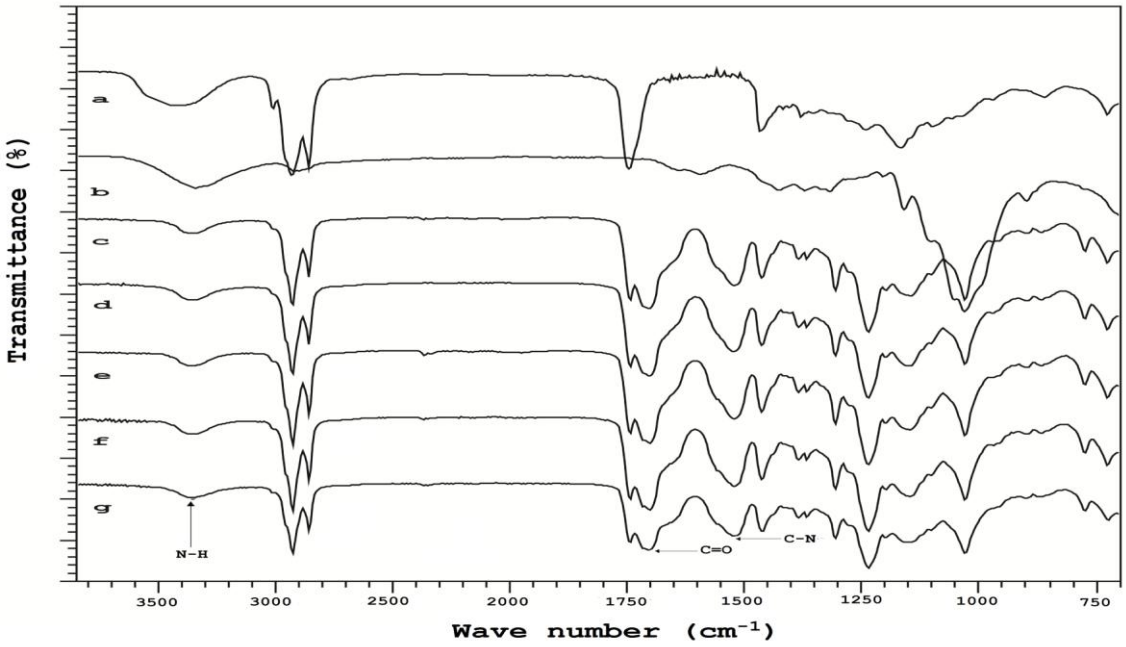

Fig.3: ATR-FTIR spectra of **CO** (a), cellulose (b), **IPU100** (c), **IPU90**(d), **IPU80**(e), **IPU70**(f) and **IPU60** (g).

Table 3: Wave numbers of N-H elongation obtained by FTIR analysis of composites.

Composite	N-H elongation wave number (cm^{-1})
IPU100	**3360**
IPU95	**3357**
IPU90	**3356**
IPU85	**3353**
IPU80	**3350**
IPU70	**3346**
IPU60	**3341**

3.2. Thermal properties:

DSC and **TGA** analyses are two techniques widely used in the study of thermal properties of polymers and composite materials [26]. The **DSC** thermograms of IPU100, cellulose and their composites were obtained by analyzing the samples at a heating rate of 10°C/min. All the samples show a single glass transition temperature which suggests compatibility between the matrix and cellulose fibers [27]. The T_g of **IPU100** is determined to be about 10.1°C. From the results listed in Table 4, it can be seen that the increase in cellulose percentage in the composites leads to an increase in T_g.

Table 4: T_g values of the prepared composites.

Composites	T_g (°C)
Cellulose	30
IPU100	10.1
IPU95	11.7
IPU90	12.2
IPU85	13.4
IPU80	14.3
IPU70	15.8
IPU60	17.7

This result is generally attributed to the existence of interactions between the components of polymers blends that are presently, the polyurethane matrix and the cellulose fibers [23]. Such interactions can be of physical nature such as hydrogen bonding as previously revealed by FTIR studies (i.e: the donor being NH group of the urethane linkage and the acceptor may be either the hard segment of polyurethane matrix or the alfa cellulose

fibers) [28], or of chemical nature from the reaction of hydroxyl functions in cellulose fibers with the remaining isocyanate groups during the polymerization process.
The TGA thermograms given in Fig.4, were recorded between 25 and 700°C under nitrogen at a heating rate of 10°C/min. The curves show the weight losses of **CO**, cellulose and **IPUi** versus the temperature. The degradation of **CO** occurs on one step from 320 to 480°C. Its residual mass is about 1.10%. Cellulose fiber thermogram shows a unique decomposition step after humidity release (4.2%) at around 80°C. This step takes place at 160°C and the residual mass is found to be 35%.

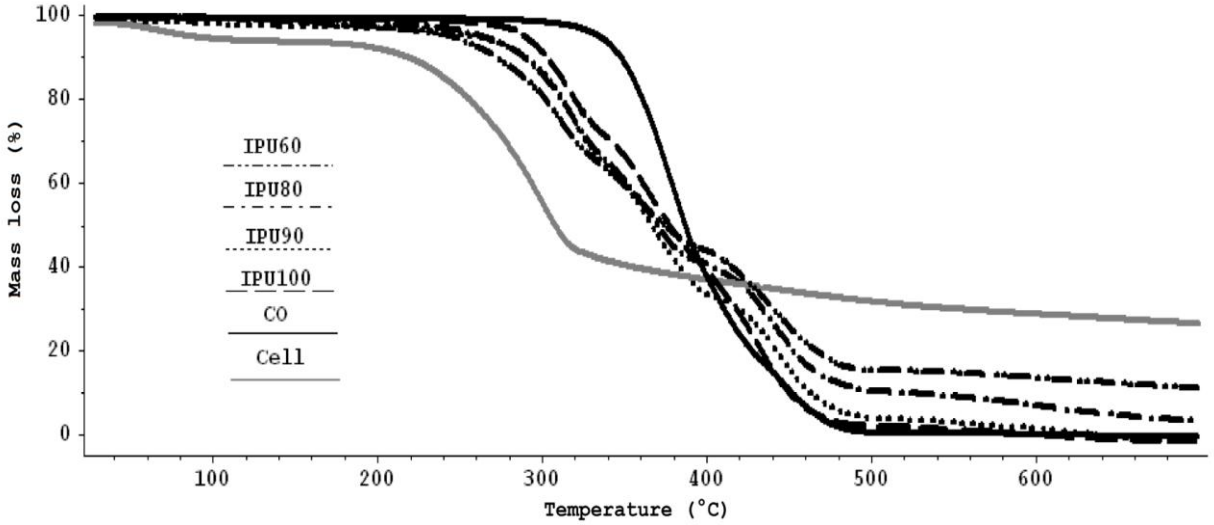

Fig.4: TGA thermograms of **CO**, cellulose and **IPUi**.

The thermal degradation of polyurethanes occurs as a result of a multitude of physical and chemical phenomena [29]. In the case of **IPU100**, the decomposition process is characterized by a first weight loss at a temperature around 265°C which arises due to the primary fragmentation of the urethane linkage and the ester groups. This decomposition process results in the formation of isocyanate, alcohol, primary or secondary amine, olefin and carbon dioxide [30-31]. The second stage corresponds to the decomposition of the soft segments at 330°C for **IPU100**. The last stage is the degradation of the remaining **CO** structures and the C—C bond cleavage at 400°C leading to a residual mass of 0.2%.
The incorporation of cellulose fibers in these matrices decreases the thermal stability of the pure PU below 380°C. Indeed, the first decomposition stage of the composites starts at lower temperatures than that of the pure **PU**. Nevertheless, at temperatures higher than 380°C, the presence of natural fibers delays the decomposition of **PU** by forming a protective layer which slows down its degradation [20]. Consequently, the thermal stability of the composites is enhanced with the increase in fiber percentage.

3.3. Morphology of IPUi:
The prepared samples were analyzed by **SEM**. The films were immersed in liquid nitrogen and then manually broken. The recorded images are given in Fig.5. It can be seen that the **IPU100** film (Fig.5a) is homogeneous and the lamellar arrangement may be unexpectedly induced by the fracture process[20]. The micrographs of composites (Fig.5 b and c) show that the cellulose fibers are randomly embedded in the matrix. The presence of **PU** at the fiber surfaces indicates enhanced compatibility between polyurethane matrix and cellulose fibers at interface due to hydrogen interaction and possible covalent bonding[6, 32]. At higher cellulose loading (more than 20%), microvoids are observed in the fractured surfaces and a part of cellulose fibers were pulled out from the matrix in the fracture surface. This is generally attributed to the aggregation of cellulose fibers and an increase in the discontinuity between polymer matrix and cellulose fibers in the composite.

3.4. Mechanical properties:
To study the effect of cellulose content on the mechanical properties of the composites, samples of H3 type geometry prepared according to ISO 37 norms were submitted to axial traction. Young's modulus was calculated from the linear part of the stress-strain curves. The obtained results are grouped in Fig.6 and Table 5.

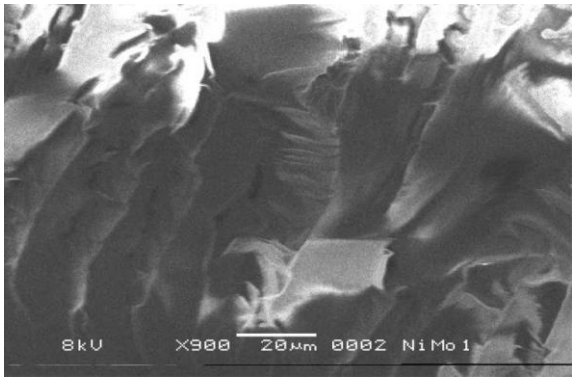

a)

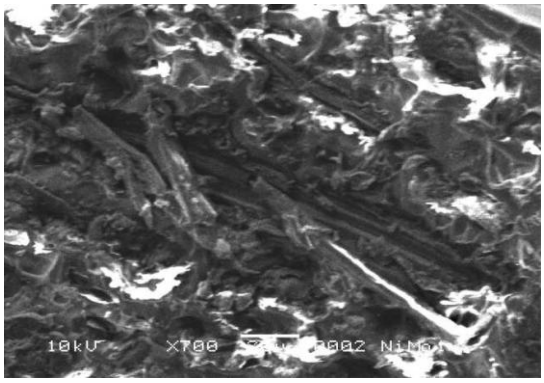

b)

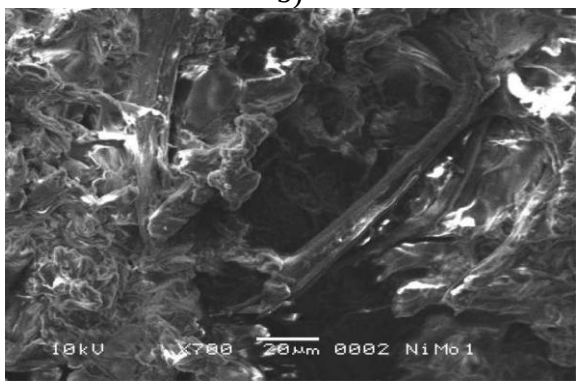

c)

Fig.5: SEM Images of **IPU100** (a), **IPU70** (b) and **IPU60**(c).

Table 5: Tensile strength, elongation at break an Young's modulus of **IPUi**.

Composite	Tensile strength (MPa)	Elongation at break (%)	Young's Modulus (MPa)
IPU100	27.9	450.4	4.9
IPU95	7.7	272.9	5.1
IPU85	9.2	233.5	6.9
IPU80	10.1	202.5	10.6
IPU70	7.5	169.6	18.9
IPU60	5.9	123.7	24.7

It can be seen that **IPU100** shows an elastic behavior before rupture. The elongation at break is about 450% at a tensile strength (σ_B)= 28MPa while the Young's modulus (E) values is 5 MPa. This low modulus value is typical of elastomer polymers [33]. The incorporation of cellulose fibers reduces the elasticity of the matrix and hence their elongation at break. Indeed, the elongation at break decreases from 450% to 123% for IPU100 and IPU60, respectively. These results are consistent with the existence of chemical bonding and hydrogen interactions between polymer matrix and hydroxyl functions of cellulose fibers [33].

Fig.7 and 8 show the effect of the cellulose fiber content on Young's modulus and tensile strength of the composites respectively. The Young's modulus increases linearly with cellulose fibers loading but follows two distinct slopes: the first interval up to 15% of cellulose fibers content shows a slow slope, while the second interval, from 15% to 40% of cellulose fibers content, shows a relatively higher slope. This is probably due to morphological changes of the composites at higher content of cellulose fibers and lower polymer content. Such changes are generally responsible for weaker mechanical properties of the composites and can be induced by the aggregation of cellulose fibers and the formation of microvoids [34] which result in the decrease in stress transfer efficiency between the polymer matrix and cellulose fibers.

These morphological changes are also depicted through tensile strength curve (fig.8) where a slow and linear increase of the tensile strength is observed in the interval from 5% to 20% of cellulose fibers content. At higher cellulose content (from 20% to 40%) the tensile strength decreases. It should be however noticed that the incorporation of cellulose fibers in the matrix reduces dramatically the tensile strength which slows down from 28 MPa for IPU100 to limited values, between 5 and 10 MPa, for the prepared composites.

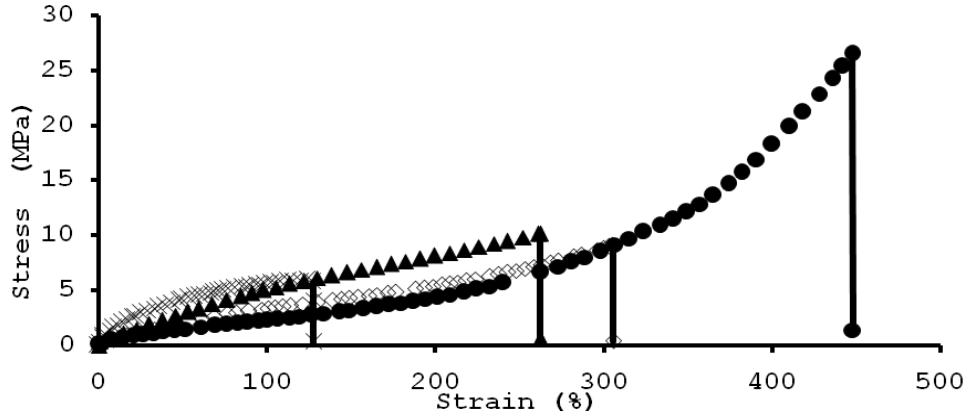

Fig. 6: Stress–strain curves of **IPU100** (●), **IPU95** (◇), **IPU85** (▲) and **PIPU60** (×).

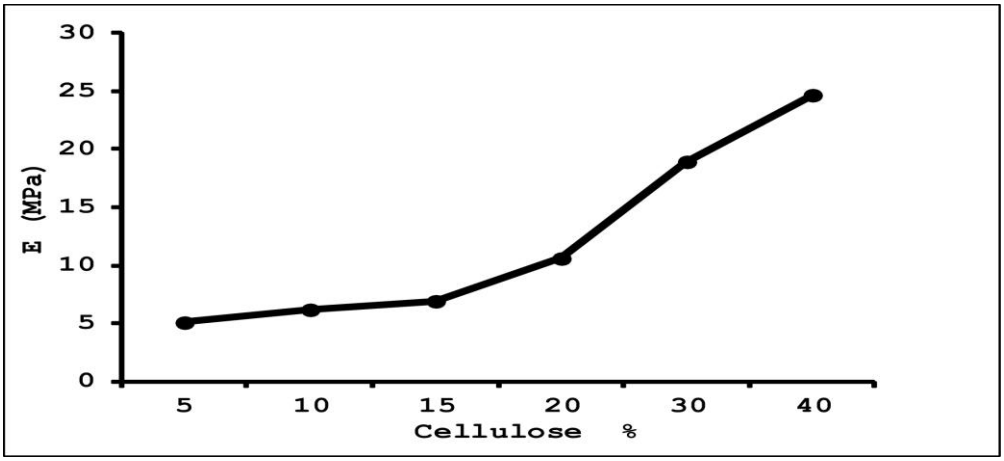

Fig. 7: Young's modulus of **IPUi** versus cellulose fibers percentage.

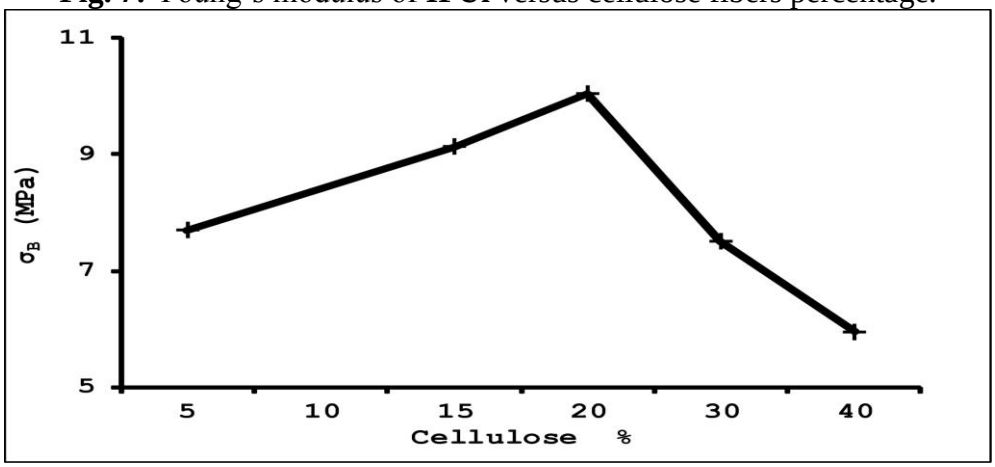

Fig. 8: tensile strength of **IPUi** versus cellulose fibers percentage.

3.5. Physico-chemical properties:

4.5.1. Water uptake test:

The water absorption results are crucial for understanding the performance of cellulose-based composites, since the moisture pickup under immersion in water or exposure to high humidity, intimately relates to such composite properties as mechanical strength, dimensional stability and appearance [35]. Fig.9 shows the water uptake versus time for **IPUi** composites. All the composites absorbed water during the experiment, but following quite different profiles. Since **IPU100** is of a hydrophobic nature **WU**$_\infty$(**IPU100**) ≈ 2%), the water uptake of the composites was entirely due to the presence of natural fibers known to be hydrophilic [36]. In fact, the water uptake rises as follows: **WU**$_\infty$(**IPU95**)=3.33%, **WU**∞(**IPU80**)=10% and **WU**∞(**IPU70**)= 47.5%

and **WU**∞(**IPU60**)=64%. The increase in **WU** with increasing fiber content in composites is common for cellulose fiber-filled composites [37].

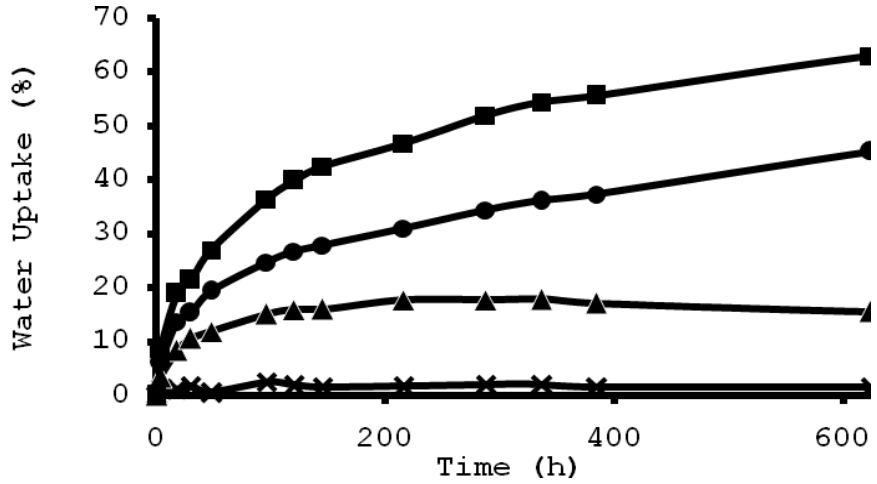

Fig. 9: Water uptake versus time of **IPU100** (x), **IPU90** (▲), **IPU70** (●) and **IPU60** (■).

These results could be confirmed by the endothermic peaks that appear within the range 50–140 °C in the **DSC** curves obtained from the first scan, which are caused by the evaporation of the moisture absorbed from the environment. Peak temperature and enthalpy value of the endotherms related to moisture evaporation are listed in Table 6.

Table 6 : Peak temperature and enthalpy value of the endotherms related to moisture evaporation from the first scan DSC thermograms of IPUi and cellulose.

Composite	Temperature (°C)	Enthalpy (J/g)
IPU100	83.4	2.011
IPU95	104.3	19.77
IPU85	116.9	27.83
IPU80	123.8	24.97
IPU70	139.6	40.34
IPU60	136.9	52.55
Cellulose	110.8	231.3

Water evaporation takes place at higher temperatures and the water evaporation enthalpy increases when the cellulose content increases in the **PU** matrix, confirming that the moisture content of the composites increases with the cellulose fiber amount and the water molecules are strongly bonded to the hydrophilic fibers [38].In fact an increase in fiber loading is known to increase the number of hydroxyl groups as well micro-voids in the composites.

3.5.2. Contact angle measurement:

Contact angles can be measured on a macroscopic level to characterize the average wettability of materials. On a microscopic level, contact angles probe the physics and chemistry of the microscopic region near the contact line [39]. The contact angle average value of a micro water drop on the surface of **IPU100** after 60 seconds of deposition is about 61.2°. Figure 10 shows the values of contact angles of composites for a period of 100 ms. It can be seen that the average values of contact angles increase with the increasing cellulose fiber amount and suggests an increase in hydrophobic character of the composite surface with cellulose content. Water uptake studies showed, however, that the cellulose fibers enhance the hydrophilicity of composites.

These contradictory results, clearly illustrate the nature of the physicochemical phenomena involved in each case. While the former depends on the surface nature and is measured over short time intervals, the later is a thermodynamic phenomenon that tends to equilibrate over time. Therefore, contact angle measurements can only characterize the surface aspect of the materials while water uptake is a bulk property.

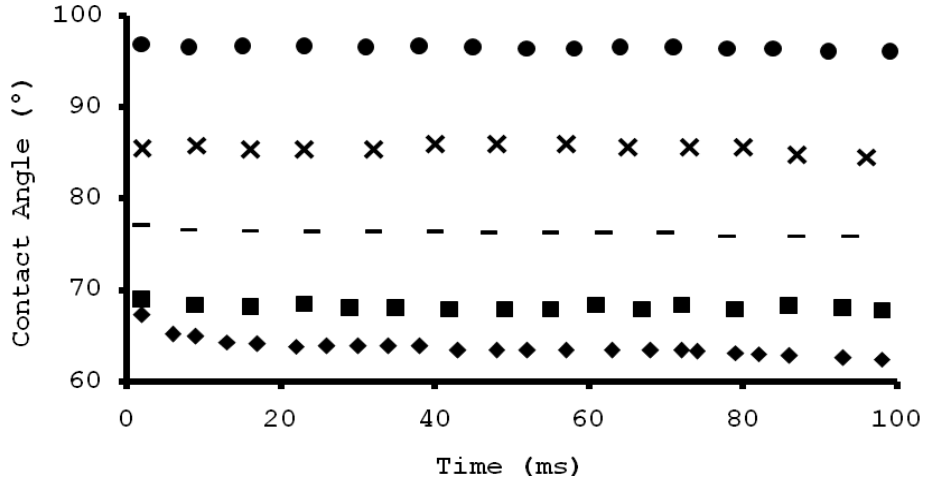

Fig. 10: Contact angle versus time of **IPU100** (♦), **IPU95** (■), **IPU80** (-), **IPU70** (x) and **IPU60** (●).

The higher contact angle of cellulose-**IPU** composites recorded may be due to thorough encapsulation of cellulose fibers in the **IPU** matrix due to the existence of chemical and physical interactions Fiber/Matrix. Consequently, the encapsulation decreases the number of hydroxyl groups responsible for the hydrophilic nature of the cellulose fibers [40]. This result agrees with the **SEM** micrographs analysis where it has been observed that the cellulose fibers are embedded inside the matrix. Also, the effective bonding between the OH groups of the cellulose fibers and the –NCO or –NH functions of polyurethane results in the formation of crosslinked polymer composite with a highly hydrophobic surface.

3.5.3. Swelling test in toluene:

Swelling test in organic solvents is a simple and efficient method to elucidate the crosslinking density of polymers. Greater is the crosslinking density lower will be the swelling rate. The samples were submitted to a swelling test in toluene. The results are shown in Fig 11.

The curves exhibit clearly two separated zones. The first one takes place at the beginning of the test, and is characterized by a rapid kinetics of swelling solvent absorption. The second zone is much slower and leads to a plateau. It's also noticed, that the swelling percentage is reduced by increasing fiber content which is due to strong linkage between the PU matrix and the cellulose fibers by both hydrogen bonding and possible chemical bonding leading to enhanced crosslinking density [25].

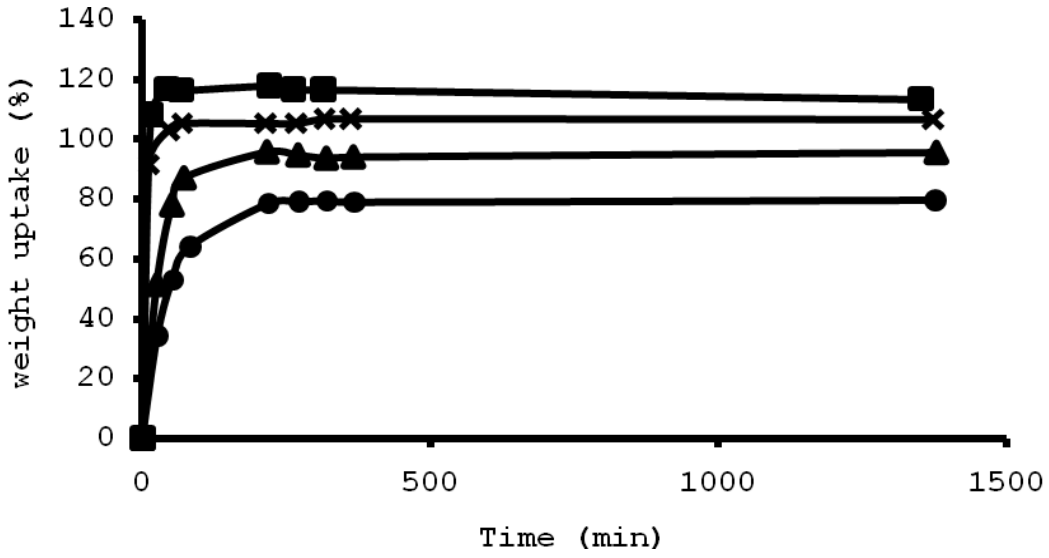

Fig.11: Toluene uptake versus time of **IPU100** (■), **IPU95** (x), **IPU70** (▲) and **IPU60** (●).

Conclusion

This study explored the development of composite materials from renewable resources. Natural fiber-reinforced polyurethane composites were prepared by mixing cellulose fibers extracted from alfa stems and castor oil-based polyurethane matrix. The FTIR spectra revealed the presence of hydrogen interactions between cellulose fibers and the **PU** matrix. The thermal stability of the composites was intermediate between that of cellulose fibers and polyurethane matrix. The increase of T_g values with increasing fiber content was interpreted by the existence of strong hydrogen bonding at the interface between fiber and matrix.

The mechanical testing showed that Young's modulus of the composites increase linearly in two slopes with fiber loading, while tensile strength increased up to 20% cellulose fibers content and decreased for higher cellulose fibers content. The weaker mechanical properties obtained for cellulose content higher than 20% were interpreted by morphological change of the composite structure due to the the existence of microvoids and aggregation of the cellulose fibers in the PU matrices. Moreover, contact angle and water uptake measurements showed that the composite surface becomes more hydrophobic, while, the water uptake of composites increases with increasing cellulose fibers content. These results have been interpreted as the consequence of different physico-chemical phenomena involved in each case.

References

1. Raquez, J.M., Deléglise, M., Lacrampe, M.F., Krwaczak, P. *Prog. Polym. Sci.* 35 (2010) 487.
2. Satyanarayana, K.G., Arizaga, G.G.C., Wypych., F. *Prog. Polym. Sci.* 34 (2009) 982.
3. Satheesh Kumar, M.N., Manjula, K.S., Siddaramaiah. *J. Appl. Polym. Sci.* 105(6) (2007) 3153.
4. Teramoto, N., Saitoh, Y., Takahashi, A., Shibata, M. *J. Appl. Polym. Sci.* 115 (2010) 3199.
5. Sharma, V., Kundu, P.P. *Prog. Polym. Sci.* 33 (2008) 1199.
6. Melo, B.N., Pasa, V.M.D. *J. Appl. Polym. Sci.* 89 (2003) 3797.
7. Othmer, K. In Encyclopedia of Chemical Technology. 5. John Wiley & Sons. New York. 1979.
7. Ogunniyi, D.S. *Bioresour* 97 (2006) 1086.
8. Quipeng, G., Shixia, F., Qingyu., Z. *Eur. Polym. J.* 26 (1990) 1177.
9. Xie, H.Q., Guo, J.S. *Eur. Poly. J.* 38 (2002) 2271.
10. Yeganeh, H., Mehdizadeh, M.R. *Eur. Polym. J.* 40 (2004) 1233.
11. Lyon, C.K., Garret, V.H. *J. Am. Oil. Chem. Soc.* 50 (1973) 112.
12. Somani, K.P., Kansara, S.S., Patel, N.K., Rakshit, A.K. *Int. J. Adhes. Adhes.* 23 (2003) 269.
13. Ogunniyi, D.S., Fakayejo, W.R.O., Ola, A. Iran. *Polym. J.* 5 (1996) 56.
14. Ray, S.S., Bousmina, M. *Prog. Mater. Sci.* 50 (2005) 962.
15. John M.J., Thomas S., Biofibres and biocomposites, *Carbohydr Polym* 2008; 71, 343.
16. Abdelmouleh, M., Boufi, S., Belgacem, M.N., Duarte, A.P., Ben Salah, A., Gandini, A. *Int. J. Adhes. Adhes.* 24 (2004) 343.
17. Corrales, F., Vilaseca, F., Llop, M., Gironès, J., Méndez, J.A., Mutjè, P. J. Hazard. Mater. 144 (2007) 730.
18. Taniguchi, T., Okamura, K. *Polym. Int.* 47 (1998)291.
19. Maafi, E.M., Tighzert, L., Malek, F. *J. Appl. Polym. Sci.* 118 (2010) 902.
20. Socrates, G. Infrared and Raman Characteristic Group Frequencies, Tables and Charts. 3rd Ed; JOHN WILEY & SONS. 2004
21. Paiva, M.C., Ammar, I., Campos, A.R., Cheikh, R.B., Cunha, A.M. *Comp. Sci. Technol.* 67 (2007) 1132.
22. He, Y., Zhu, B., Inoue, Y. *Prog. Polym. Sci.* 29 (2004) 1021.
23. Gironès, J., Pimenta, M.T.B., Vilaseca, F., De Carvalho, A.J.F., Mutjè, P., Curvelo, A.A.S. *Carbohydr. Polym.* 68 (2007) 537.
24. Lu, Y., Tighzert, L., Dole, P., Erre, D. *Polymer.* 46 (2005) 9863.
25. Menczel, J.D., Prime, R.B. Thermal analysis of polymers. Fundamentals and Applications. Wiley. 2009.
26. Zhang, C., Zhang, N., Wen, X. *J. Biomed. Mater. Res. Part. A.* 82A (2007) 637.
27. Mothé, C.G., de Araújo. C.R. *Thermochim. Acta.* 357-358 (2000) 321.
28. Xu, Y., Petrovic, Z., Das, S., Wilkes, G.L. *Polymer.* 49 (2008) 4248.
29. Corcuera, M.A., Rueda, L., d'Arlas, B.F., Arbelaiz, A., Marieta, C., Mondragon, I., Eceiza, A. *Degrad. Stab.* 95 (2010) 2175.
30. Chattopadhyay, D.K., Webster, C. *Prog. Polym. Sci.* 34 (2009) 1068.
31. Aranguren, M.I., Rácz, I., Marcovich, N.E.. *J. Appl. Polym. Sci.* 105 (2007) 2791.
32. Lee, S.H., Wang S. *Composites. Part. A.* 37 (2006) 80.

33. Sanadi, A.R. Natural fibers as fillers/reinforcements in thermoplastics in Introduction to Low environmental impact polymers. N. Tucker, M. Johnson, editors, U.K. Rapra Tech Ltd. 2004.
34. Freire, C.S.R., Silvestre, A.J.D., Neto, C.P., Gandini, A., Martin, L., Mondragon, I. *Comp. Sci. Technol.* 68 (2008) 3358.
35. Valadez-Gonzalez, A., Cervantes-Uc, J.M., Olayo, R., Herrera-Franco, P.J. *Composites. Part. B.* 30 (1999) 321.
37. Liu, H., Wua, Q., Zhang, Q. *Bioresource. Technology.* 100 (2009) 6088.
38. Aluigi, A., Vineis, C., Ceria, A., Tonin, C. *Composites. Part.* A. 39 (2008) 126.
39. Decker, E.L., Frank, B., Suo, Y., Garoff, S. *Colloids. Surf.* A. 156 (1999) 177.
40. Bakare, I.O., Okieimen, F.E., Pavithran, C., Abdul Khalil, H.P.S., Brahmakumar, M. *Mater. Des.* 31 (2010) 4274.